2747 23P

NASA Technical Memorandum 87322

Combined Fringe and Fabry-Perot Laser Anemometer for Three Component Velocity Measurements in Turbine Stator Cascade Facility

Richard G. Seasholtz and Louis J. Goldman
Lewis Research Center
Cleveland, Ohio

Prepared for the
67th Symposium of the AGARD Propulsion and Energetics Panel
on Advanced Instrumentation for Aero Engine Components
Philadelphia, Pennsylvania, May 19–23, 1986

NASA

COMBINED FRINGE AND FABRY-PEROT LASER ANEMOMETER FOR THREE COMPONENT VELOCITY MEASUREMENTS IN TURBINE STATOR CASCADE FACILITY

Richard G. Seasholtz and Louis J. Goldman
National Aeronautics and Space Administration
Lewis Research Center
Cleveland, Ohio 44135, U.S.A.

SUMMARY

A laser anemometer is described that was developed for use in a 508 mm diameter annular turbine stator cascade facility. All three velocity components are measured through a single restricted optical port, both within the stator vane row and downstream of the vanes. The measurements are made through a cylindrical window in the casing that matches the tip radius of the cascade. The stator tested has a contoured hub endwall that results in a large radial flow near the hub. The anemometer uses a standard fringe configuration (LFA) with a fluorescent aerosol seed to measure the axial and circumferential velocity components. The radial component is measured with a confocal Fabry-Perot interferometer. The two configurations are combined in a single optical system and can operate simultaneously. Data are presented to illustrate the capabilities of the system.

SYMBOLS

$\hat{a}_x, \hat{a}_y, \hat{a}_z$	unit vectors in Cartesian coordinate system
CFPI	confocal Fabry-Perot interferometer
d_o	diameter of probe volume between $1/e^2$ intensity points
FWHM	full-width half-maximum instrumental bandwidth of CFPI
f	focal length
f_D	Doppler shift frequency
$f_{D1,2}$	Doppler shift frequencies of light scattered from beams 1 and 2
$\vec{k}_{1,2}$	wave vectors of incident beams
k_o	wave number $(2\pi/\lambda)$
$\vec{k}_s$	wave vector of scattered light
LFA	laser fringe anemometer (AKA dual-beam laser anemometer)
P_0	inlet total pressure
$p_{h,M}$	hub static pressure at station M
$R_{1,2}$	inner and outer radii of annular clear aperture
T_o	maximum transmittance of CFPI
$\vec{V}$	velocity vector
V_{cr}	critical velocity (fluid velocity at Mach 1)
V_o	velocity magnitude
V_r	radial velocity component
V_{t_j}	measured transverse velocity magnitude
V_x	axial velocity component
V_θ	circumferential velocity component
α_j	angle between fringe normals and cascade axis (x axis)
β	one-half beam crossing angle
Δf_B	standard deviation of angular spectrum of incident beams (Eq. (15))
Δf_F	standard deviation of Fabry-Perot bandwidth
Δf_L	standard deviation of laser frequency jitter
Δf_M	standard deviation of Doppler shifted spectral peak

Δf_R	standard deviation of receiver aperture broadening (Eq. (10))
Δf_S	standard deviation of sum of broadening effects (Eq. (17))
Δf_T	standard deviation of turbulence broadening (Eq. (16))
ΔV_r	standard deviation of fluctuations of radial velocity
ϵ	deviation of mean Doppler shift from true backscatter shift (Eq. (8))
θ	angle between optical axis and flow velocity
θ_S	angle between optical axis and scattered light vector
λ	laser wavelength
σ	one standard deviation
ϕ	angle between cascade axis (x axis) and transverse velocity vector
ϕ_S	angular coordinate of scattered light vector
ψ	angular width of clear aperture in mask used to reduce spectral broadening
Ω	solid angle of collected light
$< >$	expected value operator

INTRODUCTION

Modern turbine engine designs incorporate geometries that generate highly three-dimensional flow. The accurate measurement of all three velocity components in turbomachinery research facilities is required for validation of new three-dimensional computer codes under development at the NASA Lewis Research Center and elsewhere for modeling internal flow. The well-known advantages of laser anemometry often make it the best method for obtaining these detailed measurements of internal flow fields.

The preferable approach to three-dimensional laser anemometry is to measure the three orthogonal velocity components directly (Refs. 1 and 2). This generally requires optical access from two orthogonal directions if a fringe (LFA) or two-spot anemometer is employed. Turbomachinery research facilities rarely permit more than a single (usually small) viewing port. With this typical restricted optical access, three-dimensional measurements become much more difficult (see Ref. 3 for a discussion of the problem).

The most common approach to three-dimensional measurements through a single port is to measure nonorthogonal velocity components with an LFA (or a two-spot system) (Refs. 4 to 6). However, the error of the velocity component along the optical axis obtained from this approach becomes large when the window size is small compared to the distance from the window to the measurement region. In general, it is desirable to have an angle between the axes of the LFA components of 30° or more (Ref. 7), although measurements with angles as small as 17° have been reported (Ref. 8). Thus, in spite of the advantages of the LFA technique, its limitation to the measurement of transverse components has led to the investigation of other approaches for the measurement of the on-axis component.

One approach to measuring the component along the optical axis is the reference-beam heterodyne technique. Used in a backscatter configuration, a reference-beam system directly measures the on-axis component. This method has been combined with an LFA (Ref. 9) to obtain three-dimensional measurements in a low velocity jet. However, one difficulty with using the reference-beam method in high speed flows is that the Doppler shift is about 4 MHz/m/sec for visible laser light. This results in Doppler shift frequencies that can easily exceed the frequency response of most common photomultiplier tubes. Another fundamental limitation of the reference-beam technique is expressed by the Antenna Theorem (Ref. 10), which states that the maximum effective aperture area is limited to about λ^2/Ω where Ω is the solid angle subtended by the probe volume at the receiver aperture.

Another approach for measurement of the on-axis component is the use of a high resolution optical interferometer to directly measure the Doppler shift. One example is the measurement of the optical-axis velocity component in rocket exhausts (Refs. 11 and 12). We have previously shown the feasibility of using a confocal Fabry-Perot interferometer to measure the optical-axis (radial) component in a 508 mm diameter turbine stator (Ref. 13). Also, we have described three-dimensional velocity measurements in a free jet with the Fabry-Perot in a backscatter optical configuration (Ref. 14). Other reported applications of laser anemometry with interferometers include wind tunnels (Refs. 15 to 18), an MHD generator (Ref. 19), and a plasma torch (Ref. 20).

Interferometric measurement of the Doppler shift shares with the reference-beam heterodyne technique the characteristic of providing a direct measurement of the on-axis velocity component in a backscatter optical configuration. It offers the advantage of

having essentially no upper frequency limit, which is important in high speed flows. (Actually, the use of an interferometer for low speed flows is much more difficult than for high speed flows because of the requirements of an interferometer with extremely high resolution and a laser with very good frequency stability.) Another advantage of a confocal Fabry-Perot interferometer is that the amount of usable scattered light is not limited by the Antenna Theorem, but instead by its light-gathering power (etendue). This advantage, however, tends to be offset by its relatively low transmission.

The subject of this paper is a new three-dimensional laser anemometer developed for use in the Lewis 508 mm diameter annular turbine stator cascade facility. The requirements for the anemometer were to measure the three velocity components through a single relatively small viewing port with accuracy of 1 percent of velocity magnitude and 1° of flow angles. The flow in the cascade is in the high subsonic regime with a significant radial component produced by a contoured hub endwall. (Tip endwall contouring was not used because of the difficulty of obtaining optical access for the laser system.) Furthermore, it is necessary to measure small radial velocity components in the presence of large axial and circumferential components.

Conventional fringe-type optics using fluorescent seed were selected for measurement of the transverse velocity components. This technique has previously been used at NASA Lewis for measurements in compressor rotor and turbine stator test facilities (Refs. 21 and 22). After an evaluation of the various techniques discussed above for measuring the third component (the component along the optical axis), a scanning confocal Fabry-Perot Interferometer (CFPI) was chosen.

In this paper, the Lewis turbine stator facility is briefly described. An analysis of scattering theory as it pertains to velocity measurements with an interferometer is presented followed by a description of the optical configuration of the three-dimensional anemometer. Data acquisition and processing are discussed, and some results are presented to illustrate the capability of the anemometer in the cascade facility.

EXPERIMENTAL FACILITY

Stator Cascade

The core turbine stator, full-annular cascade included an inlet section, a test section, and an exit section. A photograph and a cross-sectional view of the facility are shown in Figs. 1 and 2. In operation, atmospheric air was drawn through the inlet section, the blading, and the exit section and then exhausted through the laboratory altitude exhaust system. The cascade is described completely in Ref. 23 and briefly below.

The inlet section, consisting of a bellmouth and a short straight section, was designed to accelerate the flow to uniform axial-flow conditions at the vane inlet.

The test section, for this investigation, consisted of a sector of four vanes that were part of a full-annular ring of 36 vanes. The annular ring is shown in Fig. 3 and a schematic cross-sectional view is shown in Fig. 4. The untwisted vanes, of constant profile from hub to tip had a height of 47.625 mm at the leading edge and 38.10 mm at the trailing edge. The vane axial chord was 38.23 mm and the vane stacking axis was located at the center of the trailing-edge circle. The hub endwall contour was "s" shaped and the coordinates are shown in Fig. 4. The tip endwall had a constant diameter of 508 mm and was not contoured, as explained in the Introduction.

Cascade Flow Conditions

The test conditions in the cascade were set by controlling the pressure ratio across the vane row with two throttle valves located in the exhaust system. A hub static tap located downstream of the test section, where the flow was assumed to be nearly circumferentially uniform (station M, Fig.2), was used to set this pressure ratio. For this investigation the hub-static to inlet-total pressure ratio $p_{h,M}/P_0$ was maintained at a value of 0.724. This prevented the flow from becoming supersonic within the cascade. The design pressure ratio for the previously tested (Ref. 22) cylindrical hub endwall configuration (no contour) was 0.65 and would have produced supersonic flow within the vane passage had it been used.

Windows

A cutout in the test-section outer vane ring (Fig. 3) provided optical access. A second cutout was located downstream of the vane row. The windows were made from 3.175 mm thick window glass. They were formed into a cylindrical shape that matched the tip radius by sagging them, in a vacuum furnace, onto a machined graphite form. The vanes at the window were machined to the tip radius. A silicone rubber sealing material was used to seal both windows to the cascade housing and to seal the vane tips to the window. At the vane row, the window covered about 39° in the circumferential direction and was 4 cm high.

ON-AXIS VELOCITY COMPONENT MEASUREMENT

Scattering Theory

This section presents the theory of using the two beams of a conventional fringe-type anemometer with an interferometer to measure the on-axis velocity component.

Consider two beams with wave vectors $\vec{k}_1$ and $\vec{k}_2$ incident on a particle moving with velocity $\vec{V}$ as shown in Fig. 5. For simplicity, the beams are assumed to lie in the x-z plane and have an included angle 2β. (The fringes formed by the beams thus have normals in the x-direction as shown in Fig. 6.) The receiving optics aperture is assumed to be an annulus centered on the bisector of the beams with outer radius R_2 and inner radius R_1 and is located a distance f (the lens focal length) from the beam crossing position. The wave vector of the scattered light is $\vec{k}_s$. Thus, in Cartesian coordinates with the optical axis along the z-direction

$$\vec{k}_{1,2} = k_o \, (\mp \sin \beta \, \hat{a}_x + \cos \beta \, \hat{a}_z) \tag{1}$$

$$\vec{k}_s = k_o \, (\sin \theta_s \cos \phi_s \, \hat{a}_x + \sin \theta_s \sin \phi_s \, \hat{a}_y + \cos \theta_s \, \hat{a}_z) \tag{2}$$

$$\vec{V} = V_o \, (\sin \theta \cos \phi \, \hat{a}_x + \sin \theta \sin \phi \, \hat{a}_y + \cos \theta \, \hat{a}_z) \tag{3}$$

where $\hat{a}_i$ denotes the unit vector in the i direction and the wave number $k_o = 2\pi/\lambda$. The subscripts 1 and 2 refer to the two incident beams, and the first subscript corresponds to the upper sign.

The Doppler shifts of the light scattered in direction $\vec{k}_s$ are

$$f_{D1,2}(\theta_s,\phi_s) = \frac{1}{2\pi} (\vec{k}_s - \vec{k}_{1,2}) \cdot \vec{V}$$

$$= \frac{1}{\lambda} \left[V_t [\sin \theta_s \cos(\phi_s - \phi) \mp \sin \beta \cos \phi] + V_r \, (\cos \theta_s - \cos \beta) \right] \tag{4}$$

where $V_t = V_o \sin \theta$ is the transverse velocity component and $V_r = V_o \cos \theta$ is the component along the optical axis (the radial component in the cascade). Note that the scattered light is spread over a range of frequencies because of the finite extent of the light collecting aperture.

The mean values of the Doppler shift frequencies of the scattered light collected over the full annulus are

$$\langle f_{D1,2} \rangle = \frac{1}{\Omega} \int_{\theta_2}^{\theta_1} \int_{0}^{2\pi} f_{D1,2}(\theta_s,\phi_s) \sin \theta_s \, d\phi_s \, d\theta_s \tag{5}$$

where $\langle \; \rangle$ denotes the expected value, and

$$\Omega = \int_{\theta_2}^{\theta_1} \int_{0}^{2\pi} \sin \theta_s \, d\phi_s \, d\theta_s \tag{6}$$

is the solid angle of collected light. The limits on the integration over θ_s are given by

$$\theta_{1,2} = 180° - \tan^{-1}(R_{1,2}/f) \tag{7}$$

Carrying out the integrations, Eq. (5) becomes

$$\langle f_{D1,2} \rangle = - \frac{1}{\lambda} \left[\mp V_t \sin \beta \cos \phi + 2(1 - \varepsilon) \, V_r \right] \tag{8}$$

where

$$\varepsilon = 1 - \frac{1}{2} \left[\frac{\sin^2 \theta_1 - \sin^2 \theta_2}{2(\cos \theta_1 - \cos \theta_2)} + \cos \beta \right]$$

represents the deviation from pure backscatter and is generally $\ll 1$. If the scattered light from the two beams is of equal intensity, then the mean value of the frequency of the light scattered from both beams integrated over the annulus is

$$\langle f_D \rangle = \frac{1}{2} \left(\langle f_{D1} \rangle + \langle f_{D2} \rangle \right) = - \frac{2}{\lambda} (1 - \varepsilon) \, V_r \tag{9}$$

Thus, the mean Doppler shift is proportional to the optical-axis velocity component.

The standard deviation of the Doppler shift frequency of the scattered light is, in general, given by

$$\Delta f_R = \left\langle (f_D - \langle f_D \rangle)^2 \right\rangle^{1/2} \tag{10}$$

If the light scattered from the two beams is not of equal intensity, the terms in Eq. (8) proportional to V_t will not cancel, and $\langle f_D \rangle$ will not, in general, be proportional to V_r. However, note that if the velocity is in the y-z plane (i.e., perpendicular to the fringe normals as shown in Fig. 6), $\phi = 90°$ and the Doppler shifts of light scattered from the two beams are equal for any scattering direction. Equation (8) in this case reduces to

$$\langle f_{D1} \rangle = \langle f_{D2} \rangle = -\frac{2}{\lambda}(1 - \epsilon) \qquad V_r, \phi = 90° \tag{11}$$

Example

For the annular aperture described in the Optical Layout section,

$$\theta_1 = 176.3°$$

$$\theta_2 = 174.7°$$

$$\beta = 1.134°$$

$$\epsilon = 0.00169$$

To estimate the spectrum of the scattered light, we can let $\theta_s = 175.5°$ (since θ_s only varies over a small range) and assume that the velocity is in the y-z plane ($\phi = 90°$). Then the Doppler shift frequency given by Eq. (4) becomes

$$f_D(\phi_s) = \frac{1}{\lambda}\left[0.0785 \sin \phi_s V_t - 1.9967\, V_r\right] \tag{12}$$

The mean value of the Doppler shift is (Eq. (11))

$$\langle f_D \rangle = -\frac{1.9967}{\lambda} V_r \tag{13}$$

and the spectral width due to the receiving optics is (Eq. (10))

$$\Delta f_R = \frac{0.0785}{\lambda} \langle \sin^2 \phi_s \rangle^{1/2} V_t \tag{14}$$

For light collected over the full annular aperture, $\langle \sin^2 \phi_s \rangle^{1/2} = 1/\sqrt{2}$. For example, if $V_t = 250$ m/sec and $\lambda = 514.5$ nm, then $\Delta f_R = 27$ MHz.

Mask for Reduction of Spectral Width

A technique for reducing the spectral width caused by aperture broadening is to introduce a mask having a clear aperture angular width 2ψ as shown in Fig. 6. The mask must be oriented as shown to ensure that the mean radial velocity measurement is unbiased. An example of the spectral broadening for a transverse velocity $V_t = 250$ m/sec is shown in the following table for several masks.

ψ, deg	$\langle \sin^2 \phi_s \rangle^{1/2}$	Δf_R, MHz
30	0.294	11
45	.426	16
60	.542	21
90	.707	27

If the flow angle $\phi \neq 90°$, then the spectrum will be somewhat broader than these values.

One word of caution should be mentioned: if an angular mask is used which is not properly oriented, then the mean Doppler shift frequency will be biased. But, if no angular mask is used, the mean Doppler shift will be correct, although the spectral width will be greater.

Other Causes of Spectral Broadening

In addition to the spectral broadening discussed above caused by the spread in the wave vector of the scattered light, four other factors cause broadening. One is the

inherent instrumental broadening Δf_F. For the purposes of this paper, Δf_F is approximated by one-half of the FWHM bandwidth. (The FWHM bandwidth is given by the FSR divided by the finesse, so $\Delta f_F \cong 30$ MHz).

Another factor is jitter in the laser frequency (Δf_L), which is typically about 10 MHz in a low-noise, low-vibration environment. In a noisy environment, such as a test cell, the jitter will be greater. This jitter, of course, likewise affects the unshifted peak and the Bragg peak. A third cause of broadening is the angular spectrum of the incident beams, which is given by (Ref. 24)

$$\Delta f_B = V_t/(\pi d_o) \tag{15}$$

where V_t is the transverse velocity and d_o is the diameter of the probe volume. For this application, $\Delta f_B < 1$ MHz and therefore can be neglected.

Finally, fluctuations in the flow velocity (i.e., turbulence) cause broadening of the measured spectrum. If turbulence broadening is greater than broadening from all other effects, then the spectral width can be used as a measure of the intensity of the radial turbulence. An estimate of the intensity of the turbulence fluctuations of the on-axis velocity component is then given by

$$\Delta f_T = (\Delta f_M^2 - \Delta f_S^2)^{1/2} \tag{16}$$

where Δf_M is the measured width (1σ), and Δf_S is the sum of all other broadening mechanisms except turbulence. The various broadening mechanisms are assumed to be independent so Δf_S is given by the root-sum-square

$$\Delta f_S = (\Delta f_L^2 + \Delta f_B^2 + \Delta f_R^2 + \Delta f_F^2)^{1/2} \tag{17}$$

If, for example, the turbulence is isotropic with 10 percent intensity, the mean radial velocity is zero, and the transverse velocity is 250 m/sec, then the turbulence fluctuations of the radial velocity $\Delta V_r = 25$ m/sec and $\Delta f_T = \Delta V_r/(\lambda/2) \simeq 100$ MHz. This is larger than the broadening usually observed due to other causes; and, for this case, the measured width could be used as a measure of the turbulence intensity. In practice, the broadening due to the laser jitter and the instrumental bandwidth can be determined from the width of the spectral peak of the laser light scattered from the walls.

LASER ANEMOMETER SYSTEM

Optical Layout

A photograph of the optical system and the layout are shown in Figs. 7 and 8. The argon-ion laser was equipped with a temperature controlled etalon and had a maximum output power of 0.8 W at a 514.5 nm wavelength with a vertically polarized TEM_{oo} transverse mode and single axial mode.

Lenses L1 and L2 (focal lengths 80 and 100 mm, respectively) function as mode-matching lenses to position the beam waists at the focal plane of lens L3. The beam divider (constructed from two appropriately coated 6.35 mm thick glass plates) split the single beam into two equal intensity parallel beams (approximately 10 mm separation). The divider was mounted in a motor driven rotary mount, so the orientation of the fringes could be set at any desired angle. A half-wave retardation plate (gear driven by the mount at one-half the angle of rotation of the divider) was located at the input of the beam divider to maintain the proper linear polarization at the input of the beam divider.

The two parallel beams from the beam divider were turned by mirrors M3, M4, and M5. Mirror M4 was elliptical with a minor axis of 15.2 mm and major axis of 21.6 mm. The parallel beams were focused by lens L3 (250 mm focal length, 46 mm clear aperture) to cross at the probe volume after being reflected by mirror M5. Mirror M5 was mounted on a motor driven goniometer stage with axis perpendicular to the plane of the optical table. This enabled the optical axis to be positioned along the radial direction in the stator cascade.

The diameter ($1/e^2$ intensity) of the probe volume was about 100 μm and the fringe spacing was 13 μm (about 8 fringes). Light scattered from particles passing through the probe volume (after reflection by M5) was collimated by lens L3. An aperture mask with a central circular stop (diameter 32 mm) was used to reduce the effective length of the probe volume. This mask blocked 50 percent of the full clear aperture of the collection lens L3, which means the receiving optics had an effective f-number for light collection of f/6. The pair of lenses L4 and L5 (focal lengths 160 and 60 mm, respectively) is used to reduce the diameter of the collimated scattered light beam to 17 mm. The beam is then split with a dichroic beam splitter, which reflects 514.5 nm wavelength light and passes the longer wavelength fluorescence orange light.

After passing through a long wavelength pass filter LWF (to remove any residual 514.5 nm light), the fluorescent beam is focused by lens L6 (100 mm focal length) through a 100 μm diameter pinhole (PH) located in front of photomultiplier PMT1 (RCA

4526). The signal from this PMT is processed by a counter-type processor to provide velocity components transverse to the optical axis.

The light reflected by the dichroic beamsplitter is light elastically scattered by seed particles (i.e., not fluorescence). This 514.5 nm wavelength light is focused by lens L7 (100 mm focal length) through another 100 μm pinhole and a 16 mm focal length lens (L8, a 10X microscope objective). A narrow band laser line filter (LLF) removes any residual fluorescence and background light before the light enters the confocal Fabry-Perot interferometer (CFPI).

The CFPI has a free spectral range of 3 GHz and a maximum transmission of about 10 percent. The measured finesse (ratio of free spectral range to instrumental bandwidth) was about 50. The light exiting the CFPI was detected by photomultiplier PMT2 (RCA 8850). Photon counting electronics provided a digital count rate corresponding to the light intensity passed by the CFPI. (Additional factors to be considered in the use of a CFPI for laser anemometry are discussed in Ref. 13.)

An acoustic-optic modulator (Bragg cell) was included to generate a reference signal offset from the laser frequency by 400 MHz. The 200 MHz Bragg cell frequency was crystal controlled (the second order diffracted beam was used). This signal was used to provide a calibration signal for each sweep of the interferometer. A lens (L9) was used to collimate the beam before the Bragg cell.

Acoustic shielding was necessary to reduce vibration of the laser, which would cause a large jitter in the laser frequency. (The acoustic noise level near the cascade was measured at 105 dB.) The optics and laser were mounted in a wood box covered with a layer of an acoustical foam and lead composite. The weight of the lead shielding used was about 10 kg/m^2.

Positioning System

The laser and optics were mounted on a 610 mm by 1524 mm by 64 mm thick aluminum optical breadboard, which was mounted on a 3 axis positioning system with a 12 μm positioning accuracy and 1 μm resolution. The positioning system controller was locaated in the test cell near the cascade with an RS-232 serial communications link to the minicomputer located in the control room. In addition to the three linear stages, the beam divider and goniometer mounted mirror were also controlled with this system. This provided a sufficient number of degrees of freedom to allow the optical axis to be directed along a radial line throughout the test region.

Calibration Procedures

A critical requirement for obtaining laser anemometer data for computer code verification is the accurate determination of the probe volume location relative to the experimental hardware. For the stator cascade described in this paper, location accuracies of ± 25 μm are desired. A complicating factor in achieving this accuracy is that the stator cascade hardware moves relative to the laser anemometer when going from no-flow to flow conditions and when the ambient temperature changes. Because of these reasons, position calibration must be done under test conditions. The needed parameters are the coordinates of the cascade axis, the axial position of the leading edge of the vane row, and the circumferential location of the suction and pressure surfaces of the vanes at a given axial position.

These parameters are determined after the flow has been set to the test operation condition and has stabilized. The location of a surface is determined by scanning the probe volume through the surface and recording the intensity of the collected light. The peak in the measured intensity corresponds to the center of the probe volume being at the surface. An example of such a scan is shown in Fig. 9 for determination of the hub location. The actual peak location is estimated using a least squares fit of the data to a Gaussian as shown in the figure. By making several radial scans through the hub at different circumferential positions, sufficient data is acquired to calculate the coordinates of the cascade axis. The other parameters are determined similarly. These procedures are automatically executed to minimize the loss of test time.

A scan through a normal surface, as shown in Fig. 9, also shows the length of the probe volume. At the $1/e^2$ intensity points, the probe volume length is thus about 2.2 mm. Of course, the effective length of the measurement region can be less than this due to the signal processor threshold and the size distribution of the seed particles. In addition, the scattered light was simultaneously measured in both optical paths to verify that the probe volumes defined by the fringe and the Fabry-Perot receiving optics were located at the same position. The peak locations were within 0.25 mm.

The following procedure was used to calibrate the fringe orientation relative to the vertical axis of the positioning system. A 50 μm by 3 mm air slit was aligned parallel to the positioning system vertical axis and located about 140 mm from the probe volume. The positioning system was used to twice scan the beams horizontally across the slit. The transmitted light was recorded for each beam, and the optical system was moved vertically between the two scans so that the beams were at the same position on the slit. When the maximum light transmitted by the slit for both scans occurred at the same indicated horizontal position, the beams lay on a vertical line (fringe normals

vertical). By rotating the beams 180°, the angular rotation could also be calibrated. The goniometer stage was calibrated in a similar manner. The fringe spacing (13.0 μm) was determined from the beam crossing angle measured by scanning the two beams across the air slit with the probe volume at several distances from the slit.

Seeding

A fluorescent dye aerosol was used as the seed material for these tests. This material allowed measurements (using the technique described by Ref. 25) to be made by the LFA part of the system close to the hub, the vanes, and the windows. A liquid dye solution (0.02 molar solution of rhodamine 6G in a 50-50 mixture, by volume, of benzyl alcohol and ethylene glycol) was atomized with a commercial aerosol generator. The aerosol was injected through a 6 mm diameter tube into the flow at the entrance of the bellmouth.

The fluorescence, because it is broadband, is only usable for the fringe measurements and not for the Fabry-Perot measurements. As a consequence, transverse component measurements could be made closer to surfaces than could radial component measurements. The Fabry-Perot measurements could be made to within 3 mm of the hub. Previous work (Ref. 23) in a turbine stator cascade with a similar optical system using fluorescence allowed fringe measurements within 1 mm of the hub. Of course, it is also possible to use elastically scattered light for both the LFA and Fabry-Perot measurements. One would just substitute an ordinary beamsplitter for the dichroic beam splitter and use nonfluorescent seed.

DATA ACQUISITION

A minicomputer was used for experiment control and data acquisition. It was also used to generate on-line displays of the data so that the system could be monitored for proper operation.

Fringe Signal

The fringe signal from PMT1 was processed with a counter-type processor using four cycles of the Doppler burst. The counter output data, consisting of Doppler frequency and time-between-measurements, were transferred to the minicomputer via a DMA interface having a maximum transfer rate of about 200 kHz. Data were taken at several fringe orientations at each measurement position. For this experiment, the maximum number of fringe orientations was limited to seven by the available minicomputer memory. The fringe orientations were selected at 10° intervals and bracketed the predicted flow angle. At each fringe orientation, 1000 data pairs were taken. The frequency data (corresponding to velocity components) were stored in 256 bin histograms for later off-line processing. Typical data rates ranged from 1 to 5 kHz.

Fabry-Perot

Data from the Fabry-Perot interferometer were obtained by scanning the passband over a frequency range that included the laser frequency, the Doppler shifted frequency of light scattered from seed particles, and the Bragg shifted reference frequency. A linear ramp generator, which produced a sawtooth waveform with adjustable period, amplitude, and DC offset, was used to scan the interferometer. The data from the photon counting electronics were stored in 256 bin histograms; each bin contained the number of counts in 1/256 of the sweep duration. An adjustable number of repetitive sweeps was used to build a composite histogram. Typically, 20 sweeps of 1 sec duration were used. Each sweep was examined by the computer to determine the bin number of the peak corresponding to the Bragg reference peak. The data were then offset to place the Bragg peak at a predetermined bin. This technique was used to eliminate the effect of drift in the laser frequency for data taken over long time intervals. It was found to be desirable to take data over several seconds to reduce biasing caused by short term variations in the rate of seed particles passing through the probe volume. (The observed variation in the data rate was believed to be caused by random cross-flow at the entrance of the bellmouth where the seed was injected.)

If the radial velocity is near zero, the above technique is not applicable, but the following previously reported (Ref. 14) technique can be used. In that situation, the signal from the seed particles overlaps the zero-shift signal from the laser light scattered from the cascade walls. To extract the desired signal, two histograms are constructed: one with the seeding turned on and one with the seeding off. The histograms are subtracted during the data processing to give a difference histogram that contains only the desired signal. (Of course, the noise from the removed peaks remains.) For the result presented in this paper, this technique was not used. It would be necessary for surveys taken farther from the contoured hub.

EXPERIMENTAL RESULTS

Fringe Data

The fringe data were stored in histogram form - one 256 bin histogram for each fringe orientation at each probe volume position. A typical histogram is shown in Fig. 10. The mean velocity and flow angle of the projection of the velocity in the axial-circumferential plane were obtained using a two-step procedure. First, each of the histograms was least-squares fit to a Gaussian function to get estimates of the mean transverse velocity components V_{t_j} as a function of the fringe orientation α_j. These Gaussian histogram fits also provided estimates of the standard deviations of the flow fluctuations as a function of angle.

The second step was to determine the transverse velocity magnitude V_t and flow angle ϕ. These were found using the procedure described in Ref. 22, where V_t and ϕ are found using a least squares fit to (Fig. 11).

$$V_{t_j} = V_t \cos(\phi - \alpha_j) \tag{18}$$

The axial and circumferential components are then given by

$$V_x = V_t \cos \phi, \qquad V_\theta = V_t \sin \phi \tag{19}$$

Deviation of the data from the cosine model function provides an indication of angle biasing errors. Angle biasing is caused by a variation of data rate with flow angle, which causes the components at large angles from the mean flow direction to be biased high (Ref. 26).

In addition to the Gaussian fit, the velocity components and standard deviations were directly calculated from the histograms. The direct calculation usually gave velocity components very close (within 0.5 percent) to those obtained from the Gaussian fit, but the standard deviations tended to be larger (typically 5 to 10 percent larger). This was probably a result of stray data on the tails of the histograms. Hence, the results obtained from the Gaussian fit were used.

Fabry-Perot Data

For simplicity, no angular mask was used in the Fabry-Perot receiving optics (i.e., $\psi = 90°$), so light was collected over the full annulus. The spectral broadening due the receiver aperture is thus given by Eq. 14. Data was taken at each of the fringe orientations used for the fringe measurement; no appreciable differences was noticed in the spectral widths.

The Fabry-Perot histograms consisted of three spectral peaks (Fig. 12). The right peak is a result of unshifted laser light scattered from surfaces near the probe volume; its amplitude is a function of position of the probe volume. The left peak is the reference peak from the Bragg cell; it is shifted 400 MHz from the right peak and its amplitude could be controlled by the drive voltage on the Bragg cell. The center peak corresponds to the Doppler shifted light scattered from the seed particles. Estimates of the frequencies of the three peaks were obtained by a least-squares fit of the data to a three peak Gaussian function. The Doppler-shift frequency of the light scattered from the seed particles is thus proportional to the separation between the center and right peaks, and the mean radial velocity is then given by Eq. 9.

It is also possible to obtain an estimate of the intensity of the radial velocity fluctuations as discussed in the section Other Causes of Spectral Broadening. For this test, the width (1σ) of the non-Doppler shifted peak was about 40 MHz, which included broadening due to laser jitter and the instrumental bandwidth of the Fabry-Perot. The receiving aperture broadening Δf_R, which depends on the transverse velocity, was less than 30 MHz. Thus, the sum of all broadening effects except turbulence was less than about 50 MHz. This is less than the observed width of the Doppler-shifted peak, so an estimate of the radial component fluctuations can be calculated using Eq. 16. For the histogram shown in Fig. 12, the rms radial velocity fluctuations were approximately 7 percent of the velocity magnitude.

Survey Data

An example of the measurement of the three velocity components is shown in Fig. 13. These data show a circumferential scan between the suction and pressure surfaces of the vanes at 80 percent axial chord and 10 percent span; this location is close to the center of the contoured section of the hub where a relatively large radial velocity component exists. The figure shows data taken on two dates as well as the results of a three-dimensional inviscid computer code (Ref. 27). The DENTON computer program is a time marching finite volume solution of the Euler equations. Shown are the axial component V_x, the circumferential component V_θ, and the radial component V_r. Also shown is the velocity magnitude V_Q. These are normalized with respect to the critical velocity V_{cr} to eliminate differences due to ambient temperature changes between the measurements performed on different days.

The trends in the experimental measurements and the agreement with the theoretical calculations are quite reasonable and encouraging. However, these preliminary results are only intended to illustrate the capability of the anemometer and are not meant for code verification purposes.

CONCLUDING REMARKS

The laser anemometer described in this paper is shown as a viable means of measuring the three mean velocity components in an annular turbine stator facility. The addition of a confocal Fabry-Perot interferometer to a conventional fringe-type anemometer allowed the measurement of the radial velocity component with a backscatter configuration. The advantage of this technique compared with other methods of measuring the radial component is that it does not require a large optical access port. An important feature of the anemometer is its ability to measure a small radial velocity component when the transverse component is much larger.

The scanning Fabry-Perot interferometer used in this work for measurement of the radial (optical-axis) component does, however, have some limitations compared with fringe and two-spot anemometers used for measurement of the transverse components. These include an increased data acquisition time, an inability to measure time history data, the need for an acoustic enclosure to protect the laser from the high acoustic noise levels, and poorer performance near walls. Other applications having more generous optical access may be better served by other techniques.

REFERENCES

1. Meyers, J.F., and Wilkinson, S.P., "A Comparison of Turbulence Intensity Measurements Using a Laser Velocimeter and a Hot Wire in a Low Speed Jet Flow," International Symposium on Applications of Laser-Doppler Anemometry to Fluid Mechanics, D.F.G. Durao, ed., 1982, pp. 17.4-1 to 17.4-14.

2. Pfeifer, H.J., "A New Optical System for Three-Dimensional Laser Doppler-Anemometry Using an Argon-Ion and a Dye Laser," International Congress on Instrumentation in Aerospace Facilities, IEEE, 1985, pp. 56-62.

3. Meyers, J.F., "The Elusive Third Component," International Symposium on Laser Anemometry," A. Dybbs and P.A. Pfund, eds., ASME, 1985, pp. 247-254.

4. Johansson, T.G., et al, "A Three-Component Laser-Doppler Velocimeter," Applications of Non-Intrusive Instrumentation in Fluid Flow Research, AGARD CP-193, 1976, pp. 28-1 to 28-4.

5. Neti, S., and Clark, W., "On-Axis Velocity Component Measurement with Laser Velocimeters," AIAA J., Vol. 17, No. 9, Sept. 1979, pp. 1013-1015.

6. Sathyakumar, R., "LDV System for Three Component Measurement," U.S. Patent No. 4,263,002, Apr. 21, 1981. (Thermal Systems Inc.)

7. Orloff, K.L., and Snyder, P.K., "Laser Doppler Anemometer Measurements Using Nonorthogonal Velocity Components: Error Estimates," Appl. Opt., Vol. 21, No. 2, Jan. 15, 1982, pp. 339-344.

8. Snyder, P.K., Orloff, K.L., and Reinath, M.S., "Reduction of Flow-Measurement Uncertainties in Laser Velocimeters with Nonorthogonal Channels," AIAA J., Vol. 22, No. 8, Aug. 1984, pp. 1115-1123.

9. Orloff, K.L., and Logan, S.E., "Confocal Backscatter Laser Velocimeter with On-Axis Sensitivity," Appl. Opt., Vol. 12, No. 10, Oct. 1973, pp. 2477-2481.

10. Siegman, A.E., "The Antenna Properties of Optical Heterodyne Receivers," Proc. IEEE, Vol. 54, No. 10, Oct. 1966, pp. 1350-1356.

11. James, R.N., Babcock, W.R., and Seifert, J.S., "A Laser-Doppler Technique for the Measurement of Particle Velocity," AIAA J., Vol. 6, No. 1, Jan. 1968, pp. 160-162.

12. Morse, H.L., et al, "Development of a Laser-Doppler Particle Sensor for the Measurement of Velocities in Rocket Exhausts," J. Spacecr. Rockets, Vol. 6, No. 3, Mar. 1969, pp. 264-272.

13. Seasholtz, R.G., and Goldman, L.J., "Laser Anemometer Using A Fabry-Perot Interferometer for Measuring Mean Velocity and Turbulence Intensity along the Optical Axis in Turbomachinery," Engineering Applications of Laser Velocimetry, (H.W. Coleman and P.A. Pfund eds., ASME, 1982, pp. 93-101.

14. Seasholtz, R.G., and Goldman, L.J., "Three Component Velocity Measurements Using Fabry-Perot Interferometer," Second International Symposium on Applications of Laser Anemometry to Fluid Mechanics, 1984, pp. 8.6 to 8.12.

15. Jackson, D.A., and Paul, D.M., "Measurement of Hypersonic Velocities and Turbulence by Direct Spectral Analysis of Doppler Shifted Laser Light," Phys. Lett., A, Vol. 32, No. 2, June 15, 1970, pp. 77-78.

16. Jackson, D.A., and Paul, D.M., "Measurement of Supersonic Velocity and Turbulence by Laser Anemometry," J. Phys. E., Vol. 4, No. 3, Mar. 1971, pp. 173-177.

17. Eggins, P.L., and Jackson, D.A., "Laser Doppler Velocity Measurements in Supersonic Flow without Artificial Seeding," Phys. Lett. A, Vol. 42, No. 2, Nov. 20, 1972, pp. 122-124.

18. Jackson, D.A., and Eggins, P.L., "Supersonic Velocity and Turbulence Measurements Using a Fabry-Perot Interferometer," Applications of Non-Intrusive Instrumentation in Fluid Flow Research, AGARD CP-193, 1976, pp. 6-1 to 6-13.

19. Self, S.A., "Laser Doppler Anemometer for Boundary Layer Measurements in High Velocity, High Temperature MHD Channel Flows," Proceedings of the Second International Workshop on Laser Velocimetry, H.D. Thompson and W.H. Stevenson, eds., Purdue University, 1974, pp. 44-67.

20. Mannik, L., and Brown, S.K., "Laser Doppler Velocimetry of Particles in a Plasma Torch," Appl. Opt., Vol. 25, No. 5, Mar. 1, 1986, pp. 649-652

21. Powell, J.A., Strazisar, A.J., and Seasholtz, R.G., "Efficient Laser Anemometer for Intra-Rotor Flow Mapping in Turbomachinery," J. Eng. Power, Vol. 103, No. 2, Apr. 1981, pp. 424-429.

22. Goldman, L.J., and Seasholtz, R.G., "Comparison of Laser Anemometer Measurements and Theory in an Annular Turbine Cascade with Experimental Accuracy Determined by Parameter Estimation," Engineering Applications of Laser Velocimetry, H.W. Coleman and P.A. Pfund, eds., ASME, 1982, pp. 83-92.

23. Goldman, L.J., and Seasholtz, R.G., "Laser Anemometer Measurements in an Annular Cascade of Core Turbine Vanes and Comparison With Theory," NASA TP-2018, 1982.

24. Edwards, R.V., et al., "Spectral Analysis of the Signal from the Laser Doppler Flowmeter: Time-Independent Systems," J. Appl. Phys., Vol. 42, No. 2, Feb. 1971, pp. 837-850.

25. Stevenson, W.H., dos Santos, R., and Mettler, S.C., "Fringe Mode Fluorescence Velocimetry," Applications of Non-Intrusive Instrumentation in Fluid Flow Research, AGARD CP-193, 1976, pp. 20-1 to 20-9.

26. Seasholtz, R.G., "Laser Doppler Velocimeter System for Turbine Stator Cascade Studies and Analysis of Statistical Biasing Errors," NASA TN D-8297, 1977.

27. Denton, J.D., "An Improved Time Marching Method for Turbomachinery Flow Calculation," J. Eng. Power, Vol. 105, No. 3, July 1983, pp. 514-524.

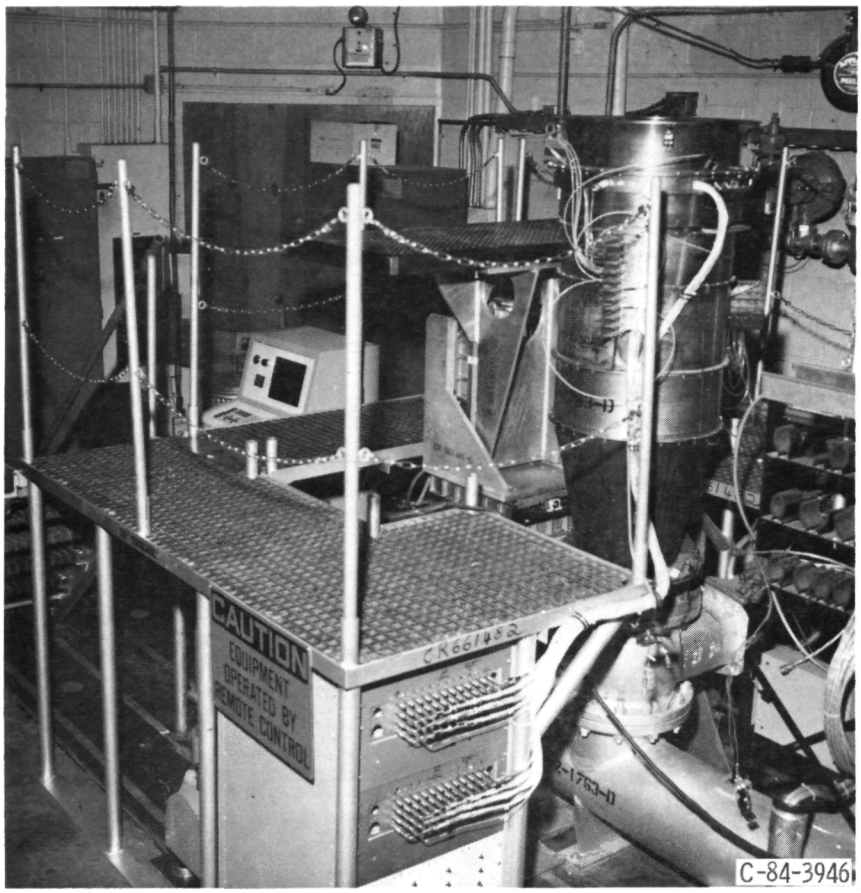

Figure 1. - Stator cascade facility.

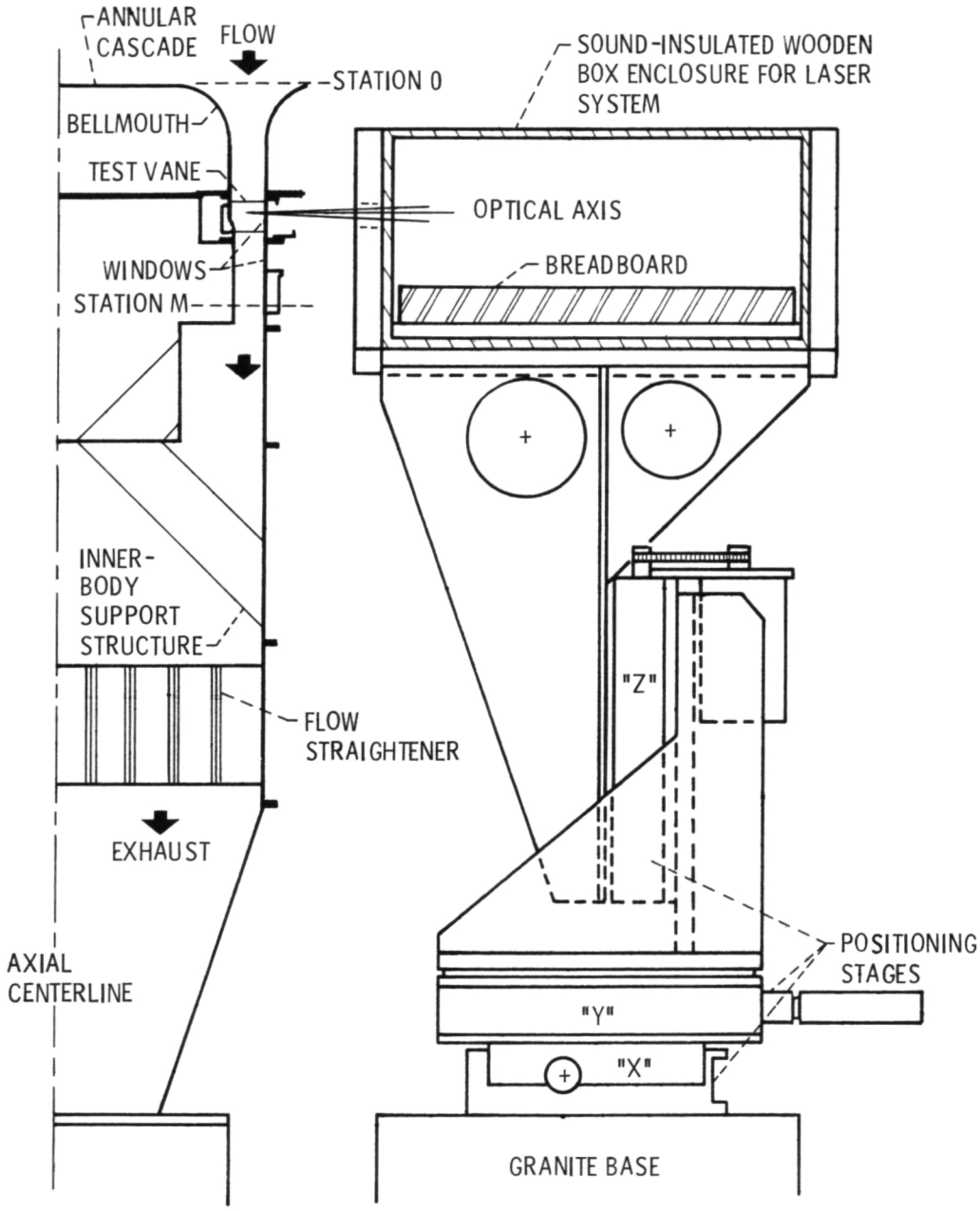

Figure 2. - Schematic cross-sectional view of core turbine stator cascade and laser positioning system.

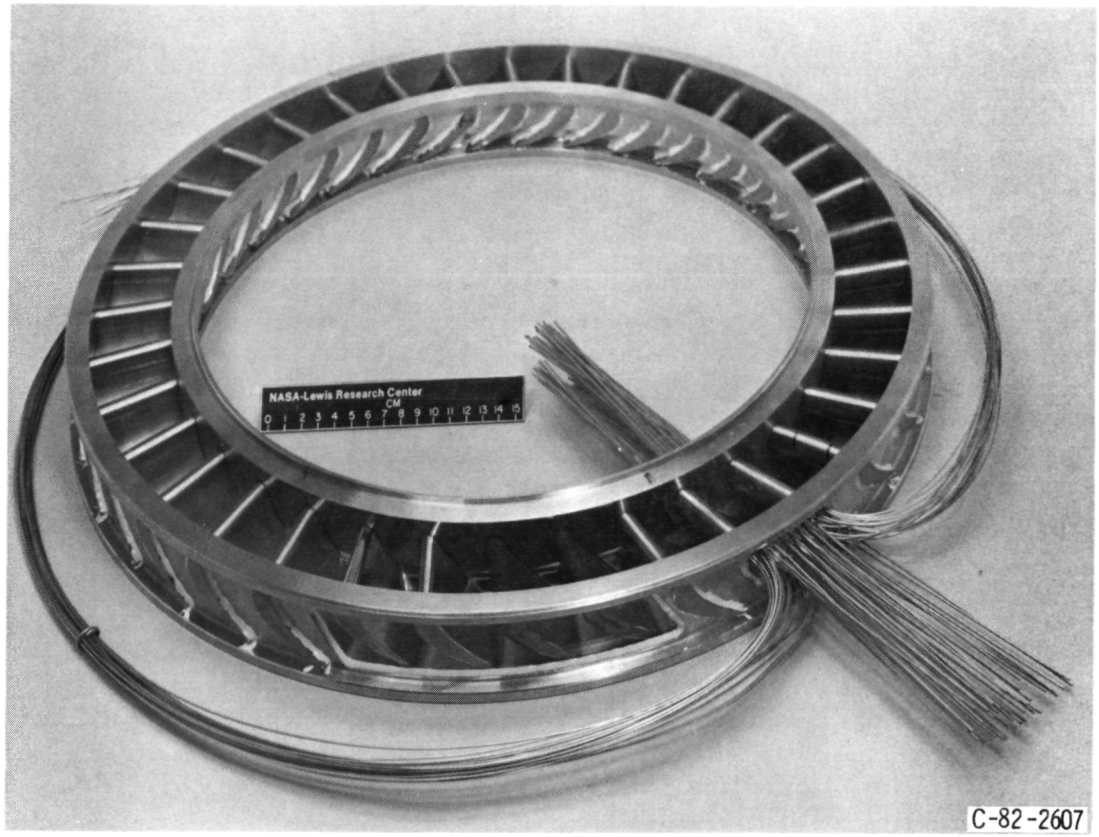

Figure 3. - Annular vane ring.

"X", mm	"Y" DIAM, mm
0.0	412.750
↓	↓
19.177	412.750
21.463	412.953
23.749	414.274
25.654	416.662
27.178	419.278
28.702	422.275
30.226	425.272
31.750	427.888
33.655	430.276
35.941	431.597
38.227	431.800

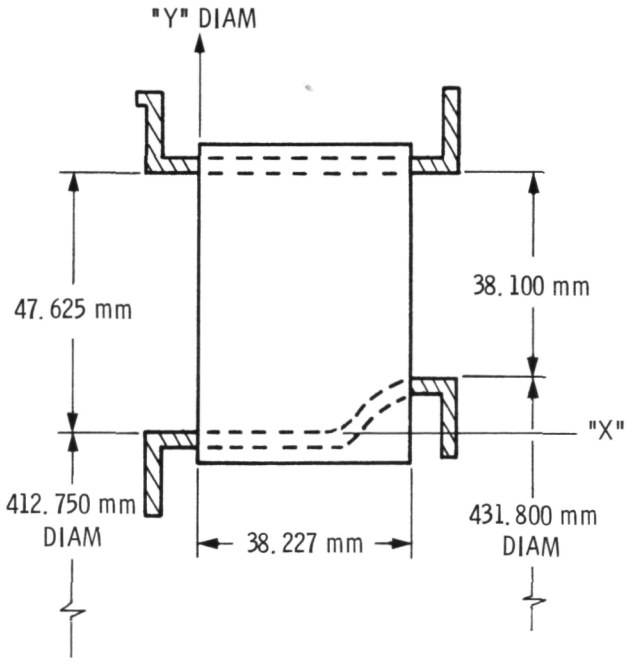

Figure 4. - Schematic cross-sectional view of contoured hub endwall vane ring.

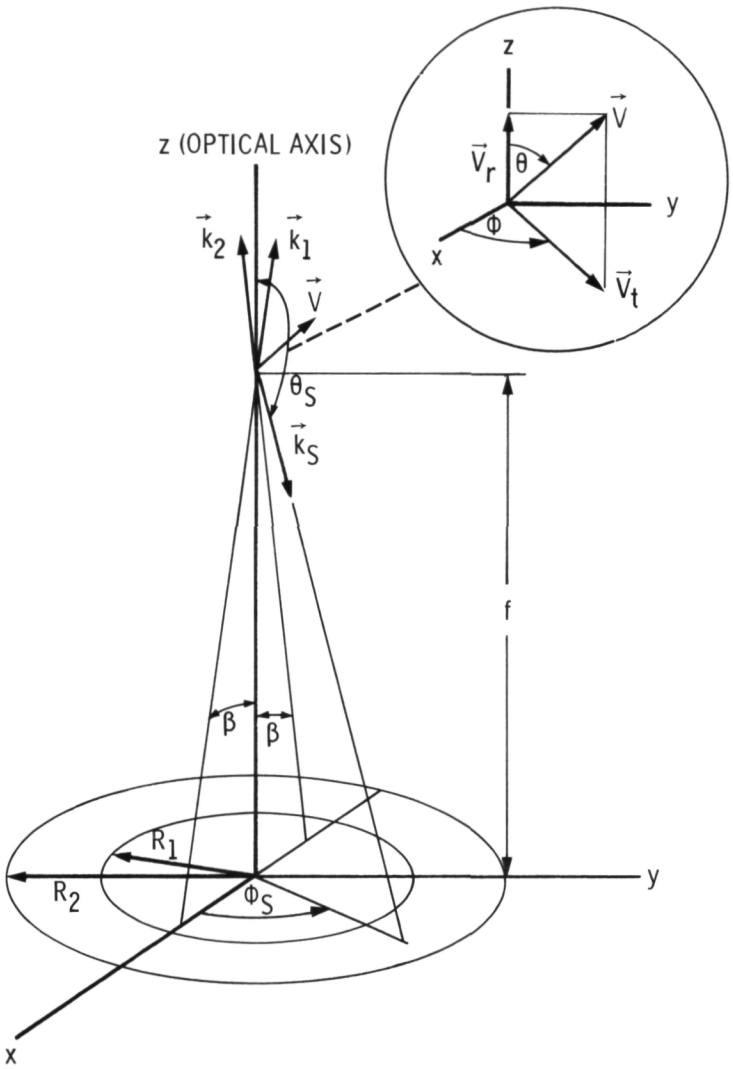

Figure 5. - Scattering geometry.

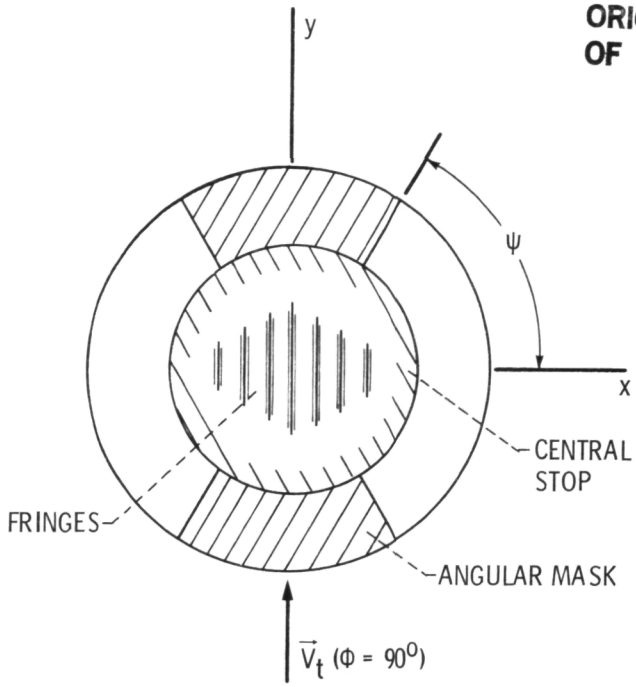

Figure 6. - Aperture mask.

Figure 7. - Three component laser anemometer.

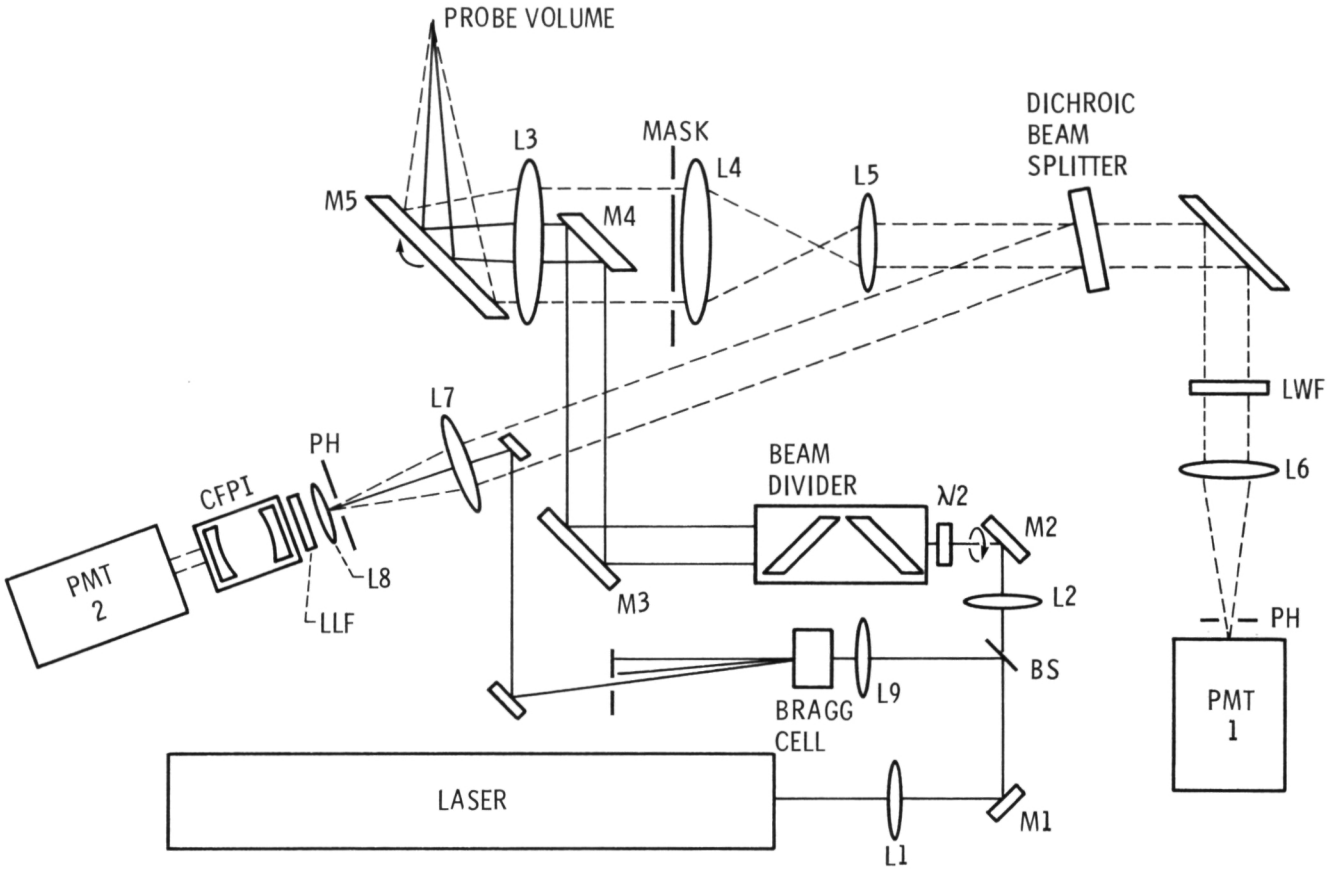

Figure 8. - Optical layout.

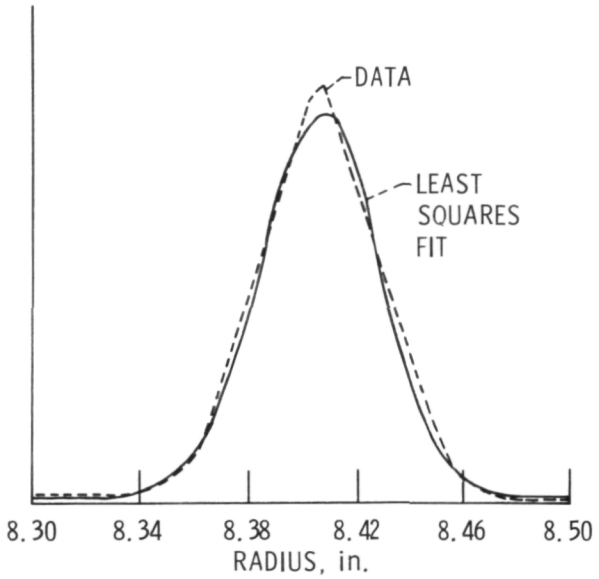

Figure 9. - Radial scan of probe volume through hub.

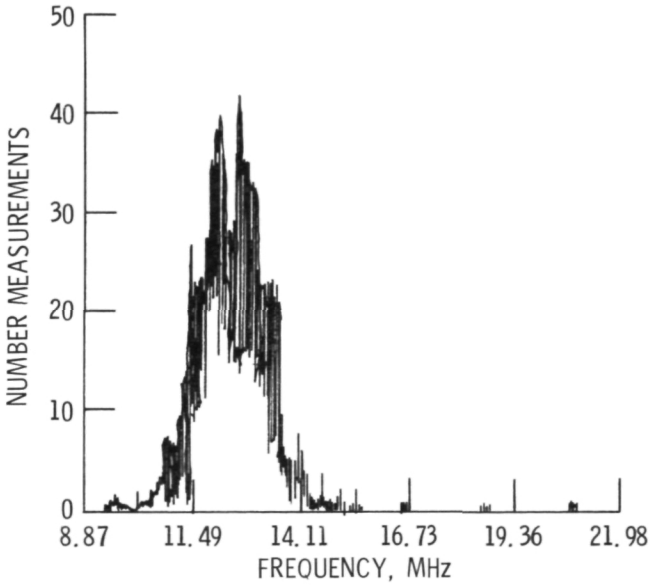

Figure 10. - Fringe data histogram.

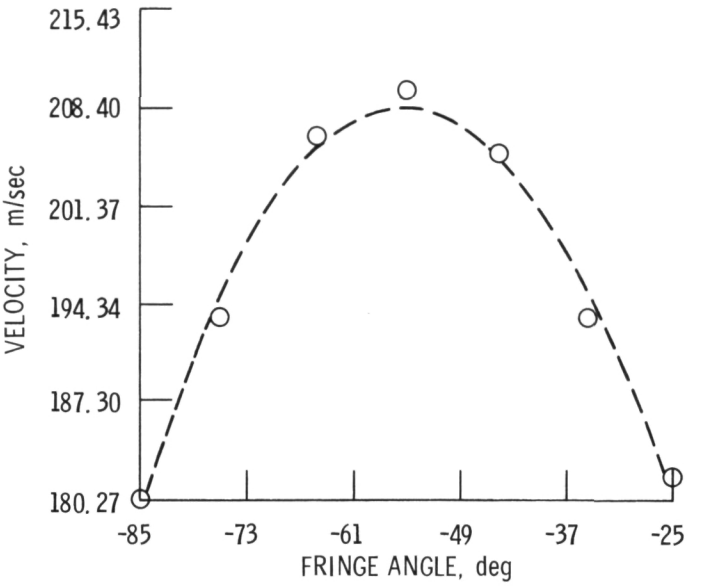

Figure 11. - Least squares fit of velocity components to cosine.

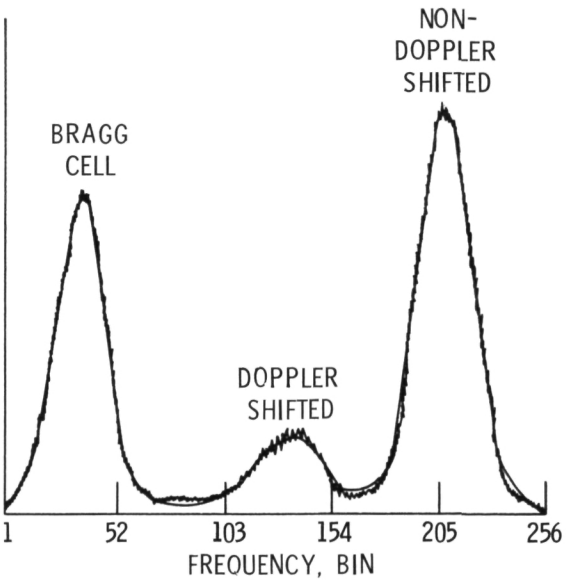

Figure 12. - Fabry-Perot spectrum.

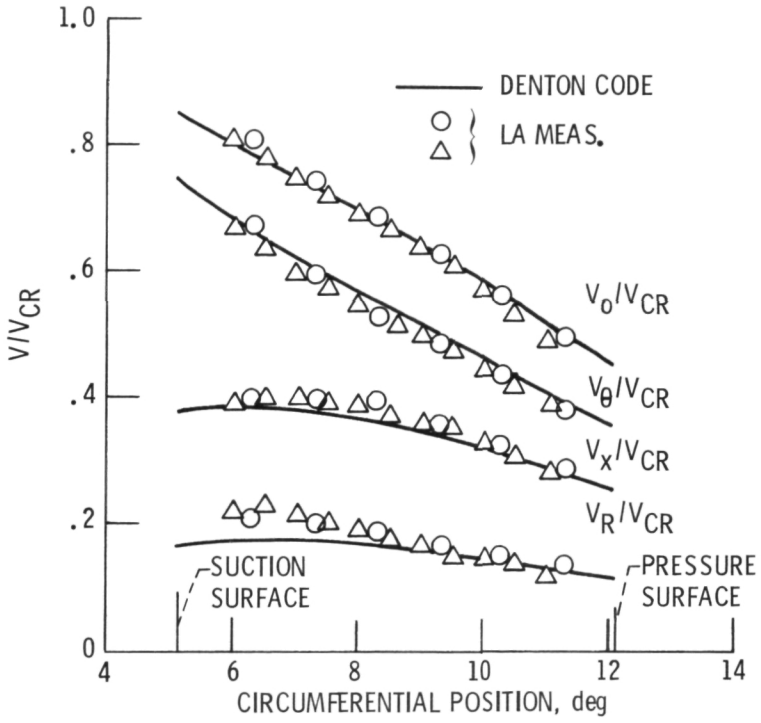

Figure 13. - Experimental survey data and Denton code results.

1. Report No.	2. Government Accession No.	3. Recipient's Catalog No.
NASA TM-87322		

4. Title and Subtitle	5. Report Date
Combined Fringe and Fabry-Perot Laser Anemometer for Three Component Velocity Measurements in Turbine Stator Cascade Facility	6. Performing Organization Code: 505-62-01

7. Author(s)	8. Performing Organization Report No.
Richard G. Seasholtz and Louis J. Goldman	E-3058
	10. Work Unit No.

9. Performing Organization Name and Address	11. Contract or Grant No.
National Aeronautics and Space Administration Lewis Research Center Cleveland, Ohio 44135	13. Type of Report and Period Covered: Technical Memorandum

12. Sponsoring Agency Name and Address	14. Sponsoring Agency Code
National Aeronautics and Space Administration Washington, D.C. 20546	

15. Supplementary Notes

Prepared for the 67th Symposium of the AGARD Propulsion and Energetics Panel on Advanced Instrumentation for Aero Engine Components, Philadelphia, Pennsylvania, May 19-23, 1986.

16. Abstract

A laser anemometer is described that was developed for use in a 508 mm diameter annular turbine stator cascade facility. All three velocity components are measured through a single restricted optical port, both within the stator vane row and downstream of the vanes. The measurements are made through a cylindrical window in the casing that matches the tip radius of the cascade. The stator tested has a contoured hub endwall that results in a large radial flow near the hub. The anemometer uses a standard fringe configuration (LFA) with a fluorescent aerosol seed to measure the axial and circumferential velocity components. The radial component is measured with a confocal Fabry-Perot interferometer. The two configurations are combined in a single optical system and can operate simultaneously. Data are presented to illustrate the capabilities of the system.

17. Key Words (Suggested by Author(s))	18. Distribution Statement
Laser anemometers Turbine Interferometers	Unclassified - unlimited STAR Category 35

19. Security Classif. (of this report)	20. Security Classif. (of this page)	21. No. of pages	22. Price*
Unclassified	Unclassified		

*For sale by the National Technical Information Service, Springfield, Virginia 22161

National Aeronautics and
Space Administration

Lewis Research Center
Cleveland, Ohio 44135

NASA